Available online at www.sciencedirect.com
ScienceDirect
Journal of Magnetic Resonance 191 (2008) 202–218
JMR Journal of Magnetic Resonance
www.elsevier.com/locate/jmr

Distance measurements in the borderline region of applicability of CW EPR and DEER: A model study on a homologous series of spin-labelled peptides

J.E. Banham [a], C.M. Baker [b,e], S. Ceola [c,1], I.J. Day [e,2], G.H. Grant [b], E.J.J. Groenen [c], C.T. Rodgers [e], G. Jeschke [d,3], C.R. Timmel [a,*]

[a] Centre for Advanced Electron Spin Resonance, University of Oxford, OX1 3QR, UK
[b] Unilever Centre for Molecular Informatics, The University Chemical Laboratory, Lensfield Road, Cambridge, CB2 1EW, UK
[c] Huygens Laboratory, Niels Bohrweg 2, 2333 CA Leiden, The Netherlands
[d] Max Planck Institute for Polymer Research, Postfach 3148, 55021 Mainz, Germany
[e] Physical and Theoretical Chemistry Laboratory, University of Oxford, Oxford, OX1 3QZ, UK

Received 1 June 2007; revised 7 November 2007
Available online 15 December 2007

Abstract

Inter-spin distances between 1 nm and 4.5 nm are measured by continuous wave (CW) and pulsed electron paramagnetic resonance (EPR) methods for a series of nitroxide-spin-labelled peptides. The upper distance limit for measuring dipolar coupling by the broadening of the CW spectrum and the lower distance limit for the present optimally-adjusted double electron electron resonance (DEER) set-up are determined and found to be both around 1.6–1.9 nm. The methods for determining distances and corresponding distributions from CW spectral line broadening are reviewed and further developed. Also, the work shows that a correction factor is required for the analysis of inter-spin distances below approximately 2 nm for DEER measurements and this is calculated using the density matrix formalism.

Keywords: DEER; EPR spectroscopy; Structure elucidation; Dipolar interactions; Spin labels

1. Introduction

Electron paramagnetic resonance (EPR) can be used to assess the distances between pairs of paramagnetic centres by relating the strength of the measured dipolar coupling to their separation. For a general review of the field for biradical systems both polarised or in thermal equilibrium see [1] and references therein. Assuming solvent-mediated superexchange and through-space dipolar interactions, the isotropic exchange coupling can be modelled approximately as a decaying exponential with inter-spin separation r, whereas the Hamiltonian for the dipolar coupling between point dipoles gives an r^{-3} dependence; for a free electron g value Eq. (1) gives the dipolar coupling frequency:

$$\nu_{dd} = \left(\frac{52.04}{r^3}\right)(1 - 3\cos^2\theta) \tag{1}$$

where θ is the angle between the inter-spin and applied magnetic field vectors, ν_{dd} is given in MHz and r is measured in nm.

This paper explores the elucidation of inter-spin distances and distance-distributions through analysis of

* Corresponding author. Fax: +44 1865 275 410.
E-mail address: christiane.timmel@chem.ox.ac.uk (C.R. Timmel).
[1] Present address: Department of Chemical Sciences, University of Padova, Via Marzolo 1, 35131 PD, Italy.
[2] Present address: Medway Sciences, University of Greenwich, Medway University Campus, Central Avenue, Chatham Maritime, Chatham, Kent, ME4 4TB, UK.
[3] Present address: Department of Chemistry, University of Konstanz, 78457 Konstanz, Germany.

1090-7807/$ - see front matter © 2007 Elsevier Inc. All rights reserved.
doi:10.1016/j.jmr.2007.11.023

1. the unresolved splitting of the X-band (~9.5 GHz) continuous wave (CW) EPR spectrum and
2. the four-pulse double electron electron resonance (DEER) signal for a series of nitroxide spin-labelled synthetic peptides in a frozen matrix.

The line broadening of the CW spectrum caused by dipolar couplings has been analysed in terms of distance and distribution previously using a variety of approaches including convolution of a relevant unbroadened EPR line shape with the dipolar spectrum corresponding to a Gaussian distribution of distances [2], Fourier deconvolution of the broadened and unbroadened spectra [3,4] and fitting the data incorporating the Euler angles of the paramagnetic centres and their spatial relationship [5]. When protonated (rather than perdeuterated) nitroxide spin probes are used, the broadening of the X-band CW EPR line shape generally becomes negligible for distances in the range of 1.5–2 nm. Broadening should not be used to estimate inter-spin distances where exchange coupling is larger than, or comparable to, the dipolar coupling term, in practice (for non-conjugated systems) this excludes distances shorter than approximately 0.8 nm.

The four-pulse DEER technique provides a deadtime-free method of measuring the frequency (i.e. strength) of the dipolar interactions [6]. In this pulsed ELDOR (ELectron DOuble Resonance) experiment, two microwave (m.w.) frequencies are applied: the first frequency provides all observer pulses whilst the second frequency is used for the pump pulse, as shown in Fig. 1 [7]. DEER has been used to measure distances from 1.6 to 7.5 nm between organic and nitroxide-based radicals [8–10]. Deadtime-free measurements allow for the determination of distance-distributions; the Matlab computer package DeerAnalysis 2006 solves the mathematically ill-posed problem of extracting distances and distributions from the DEER time domain data by Tikhonov regularisation [11–13]. The upper limit for distance measurements is imposed by the phase memory time, T_m, of the frozen sample whereas the lower limit was believed to be dictated by the excitation bandwidth of the pump pulse (which must be greater than the dipolar coupling) [14]. This work shows that the durations and non-ideality of both observer and pump pulses must be taken into account. It is demonstrated that for dipolar coupling frequencies at the limit of the excitation bandwidth, a simple correction can be made to the kernel function for Tikhonov regularisation in order to determine the distribution of inter-spin separations more accurately.

In the only previous study of nitroxide separations at the CW EPR/DEER borderline (i.e. 1–2.5 nm) of which the authors are aware, four doubly-spin-labelled mutants of human carbonic anhydrase II were investigated [15]. The distances found by CW EPR and DEER agreed well but little information about distance-distributions was given except that the DEER spectrum of one of the labelled mutants was best modelled with two distinct distances. The problem of reliable data analysis is complicated in the case of moderately broadened distance-distributions. However, spin labels often exhibit these broad distributions due to their own conformational flexibility, as well as that of the system under investigation. Uncertainties in the analysis arise because in the borderline ranges of both CW EPR and DEER the contributions from different distances are not evenly weighted. This problem is explored in more detail in the present work.

In order to carry out such an investigation, a series of peptides were designed, synthesised and spin-labelled. The peptides were based on a repeating sequence of $(AAAAK)_nA$ where n was either 4 or 7. Cysteine residues were substituted at strategic positions in the chain, in place of alanine residues, and were subsequently spin-labelled with a nitroxide-based radical. Millhauser and co-workers and Shin and co-workers used similar sequences for their CW EPR investigations into the nature of the helical secondary structure of such peptides [3,16]. The primary structures and abbreviated names of the nine peptides (eight containing two labels and one a single label) are given in Table 1.

The nine peptides were spin-labelled with MTS (1-oxyl-2,2,5,5-tetra-(methypyrroline-3-methyl)-methanthiosulfo-

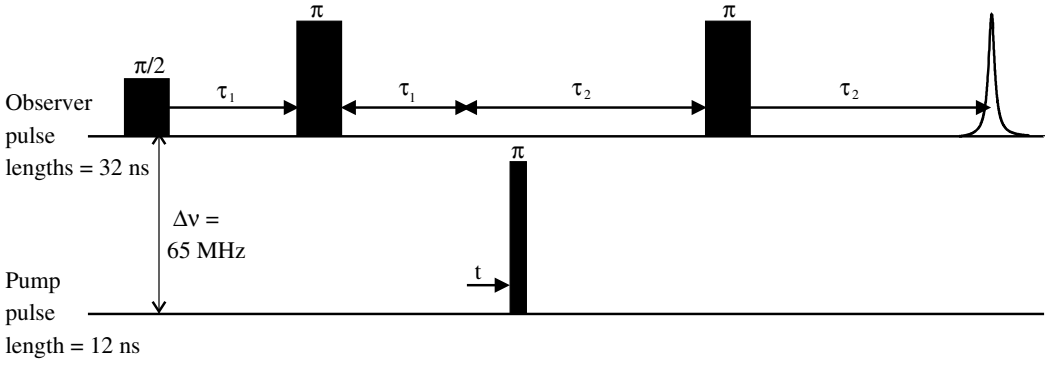

Fig. 1. EPR pulse sequence for the DEER experiment used for the work presented here. The resonator was overcoupled ($Q \sim 100$) and the pump pulse coincided with both the centre of the microwave mode of the resonator and the maximum of the nitroxide spectrum. Proton modulations were minimised by adding eight data sets with a variable delay τ_1 starting at 200 ns and using an increment $\Delta\tau_1 = 8$ ns. The t increment was 8 ns. τ_2 was between 1 and 3 μs.

Table 1
The abbreviated names and amino acid sequences for the nine investigated peptides (A, alanine; C, cysteine; K, lysine)

Name	Sequence							
	5	10	15	20	25	30	35	
4K(3)	AACAK	AAAAK	AAAAK	AAAAK	A			
4K(3,7)	AACAK	ACAAK	AAAAK	AAAAK	A			
4K(4,11)	AAACK	AAAAK	CAAAK	AAAAK	A			
4K(3,11)	AACAK	AAAAK	CAAAK	AAAAK	A			
4K(3,12)	AACAK	AAAAK	ACAAK	AAAAK	A			
4K(3,13)	AACAK	AAAAK	AACAK	AAAAK	A			
4K(3,14)	AACAK	AAAAK	AAACK	AAAAK	A			
4K(3,18)	AACAK	AAAAK	AAAAK	AACAK	A			
7K(3,32)	AACAK	AAAAK	AAAAK	AAAAK	AAAAK	AAAAK	ACAAK	A

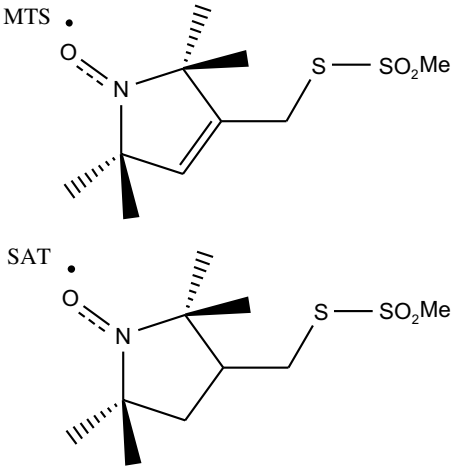

Fig. 2. The structure of the spin labels used for labelling the peptides.

nate) and the ring-saturated form which shall henceforth be referred to as SAT (1-oxyl-2,2,5,5-tetramethylpyrrolidin-3-yl-methyl)-methanethiosulfonate) (Fig. 2). The two spin labels were used in order to investigate their relative dynamic properties once attached to each peptide. While the results of these experiments are not discussed in this paper the distance results from both types of nitroxide spin label are used to show that even subtle changes in the nature of the spin label can effect the measured distance-distributions.

2. Theory and methods

This section outlines the methods of analysis used for the CW EPR and DEER data. Example results, illustrated by 4K(3,11)-MTS, are shown in Fig. 3.

2.1. CW EPR

Analysis of CW EPR spectral line broadening, caused by dipole–dipole coupling, in terms of distances and distance-distributions was carried out using custom-written programs. All techniques used the 0th harmonic spectrum which was found by integrating the experimental frequency-domain spectrum and applying a high-order polynomial baseline correction (this operation was repeated 10 times with different start and end points for the baseline correction and the average spectrum found).

2.2. Second moment analysis

The difference between the second moments of a dipolar-broadened and an unbroadened EPR line shape is directly proportional to r^{-6}. Also, the second moment of a magnetic resonance line shape is independent of isotropic exchange coupling effect [17].

The method relies on the broadening of the outer-flanks of the spectrum and thus is limited strongly by other inhomogeneous broadening effects (for example, unresolved hyperfine structure) and the quality of the baseline. The second moment of the dipolar interaction, μ_2, is obtained from the normalised dipolar broadened spectrum, d, and the normalised non-coupled spectrum, s, and is given by:

$$\mu_2 = \sum (B - \overline{B}_d)^2 d - \sum (B - \overline{B}_s)^2 s \tag{2}$$

where B is the applied magnetic field and $\overline{B}$ is the magnetic field corresponding to the mean of the spectrum [18,19]. The second moment (in Hz^2) of a powder sample of like spins is also calculated as [20]:

$$\mu_2(Hz^2) = \frac{3}{5}\frac{\mu_\beta^4 g^4 \mu_0^2}{(4\pi)^2 h^2} S(S+1) \sum \frac{1}{r^6} \tag{3}$$

The Van Vleck formula (Eq. (3)) can be converted into field units (T^2) so that Eqs. (2) and (3) can be equated and, assuming a well-defined distance, can be solved for r:

$$r(\mathrm{nm}) = \frac{2.32}{(\mu_2 . 10^8)^{1/6}} \tag{4}$$

When applying this procedure to the spectra obtained, there are two major sources of error. The first arises from the formulation of Eq. (3) which assumes like spins (i.e. strong coupling); the distance given by the second moment from coupling of unlike spins will smaller by $(3/2)^{-1/3}$. The second major error source is the polynomial baseline correction. The statistical error associated with the baseline correction can be calculated using Eq. (5) where $\sigma^d_{\mu_2}$ and $\sigma^s_{\mu_2}$ are the standard deviations in the second moment values for the doubly- and singly-labelled peptides, respec-

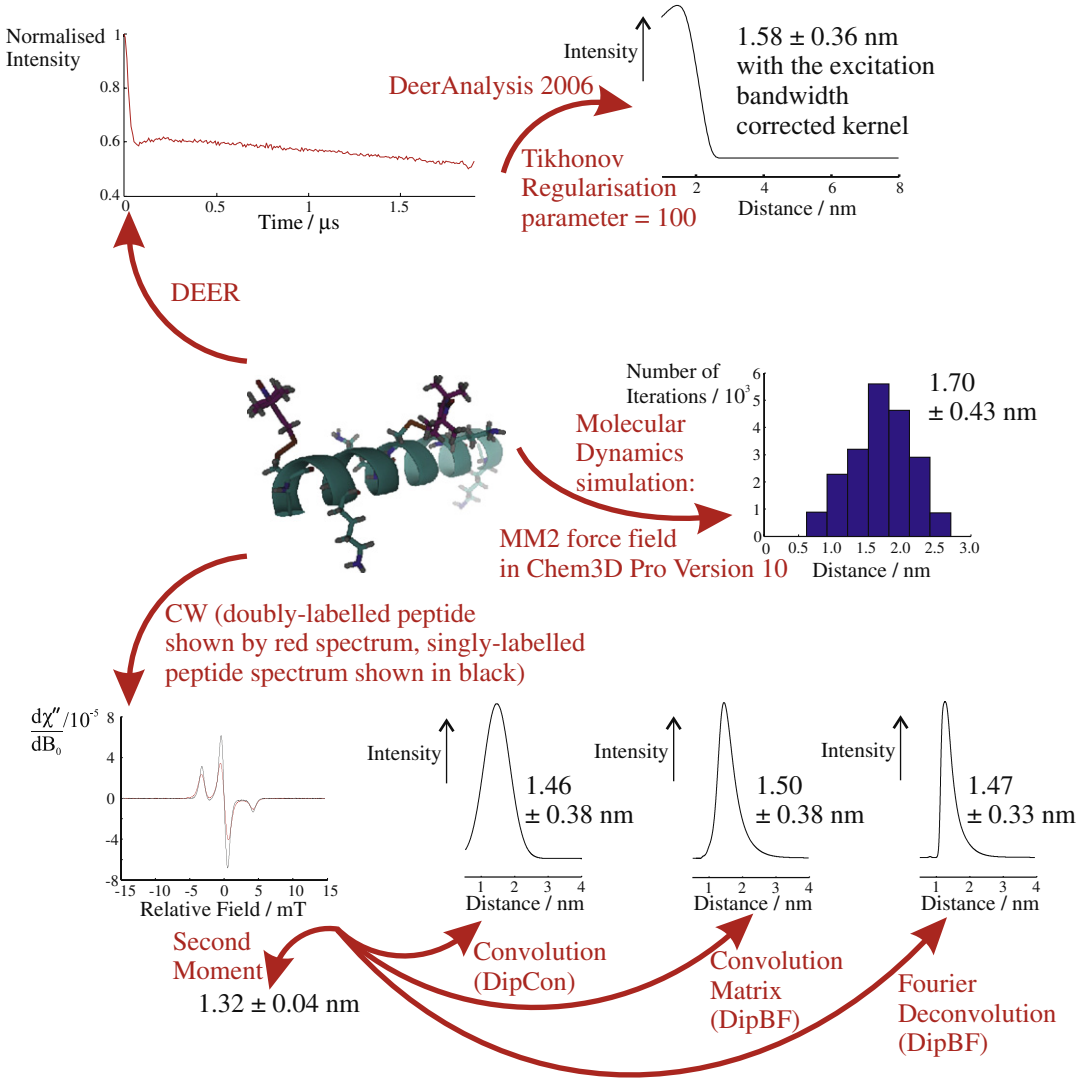

Fig. 3. The methods for finding distances and distance-distributions for a doubly-labelled peptide using EPR. The spin-labelled peptide (4K(3,11)-MTS) is shown in an α-helical confirmation. The average distance between the nitroxide moieties of the spin labels and an estimate of the distance-distribution is given by allowing movement of the cysteine side chain and spin label tether in a molecular dynamics simulation. The distance between the spin labels is measured experimentally using (i) DEER and analysis by Tikhonov regularisation and (ii) investigation of the line broadening caused by dipolar coupling in the CW spectrum (by finding its second moment, convolution, convolution matrix and Fourier deconvolution methods). For the case of 4K(3,11)-MTS, the experimental methods yield a shorter average inter-spin label distance with a smaller standard deviation than the molecular modelling for the case of a perfect α-helix. See main text for more details.

tively, for repeated data analysis with different settings for the baseline.

$$|\Delta r| = 0.044\mu_2^{-7/6}\left[(\sigma^d_{\mu_2})^2 + (\sigma^s_{\mu_2})^2\right]^{1/2} \quad (5)$$

For a given biradical it is difficult to assess the contributions from like and unlike spins and therefore Eq. (4) was used without modification. The two main sources of error are likely to be about the same magnitude and both will increase with radical separation.

2.3. Convolution

The dipolar broadened EPR spectrum can be considered as a sum of non-coupled (singly-labelled) species convolved with an appropriate dipolar broadening function. Assuming that this function is formed from a superposition of Pake patterns, the coupled (doubly-labelled) spectrum can then be reconstructed. The Pake, or dipolar coupling, pattern is formed from random orientation distributions (isotropic θ in Eq. (1)) of dipole–dipole interacting spins (nuclei or radicals) [21]. The minimum intensity will occur when $\nu_{dd}(\theta = 0 \text{ radians}) = \nu_{\|}$ (the vector connecting the spins is parallel to the magnetic field) while the maximum will be when $\nu_{dd}(\theta = \pi/2) = \nu_{\perp}$ (the vector connecting the spins is perpendicular to the magnetic field). The form of the pattern depends upon the model used for the relationship between the exchange and dipolar coupling interactions. If the difference between the Larmor frequencies of the coupled spins is much greater than the difference

between the exchange and dipolar coupling, the weak coupling regime is encountered and the turning points are dependent upon J (the magnitude of the exchange interaction) as well as v_{dd}. When the difference between the exchange and dipolar coupling frequencies is much greater than the frequency difference between the spins, the system is strongly coupled and the dipolar frequency pattern is independent of J. For nitroxide radicals at X-band EPR frequencies (i.e. 9.5 GHz) the spectral width is of the order of 180 MHz which indicates that strong coupling can be assumed for the CW EPR lineshape analysis for inter-spin separations below approximately 0.7 nm whereas the weak coupling case is appropriate for distances greater than approximately 1.5 nm, provided that J is almost negligible (which is usually true for non-conjugated systems with inter-spin separations greater than 0.8 nm) [22,23]. As mentioned in Section 2.2 above, the dipolar coupling splitting is 3/2 times larger for the strong coupling regime than for weakly coupled spins. The region between 0.7 and 1.5 nm is not adequately described using either strong or weak coupling which can cause problems for the analysis of most CW EPR dipolar broadened spectra.

Steinhoff and co-workers have developed a Fortran 77 program, "Dipfit", which simulates the non-coupled spectrum [2]. This is then convolved with a sum of Pake patterns in the strong coupling regime, corresponding to a Gaussian distribution of distances until the sum squared residual between the experimental and simulated spectrum is minimised. A custom-written version of the convolution program was produced using Matlab 7.0, and shall henceforth be referred to as "DipCon". This program uses the simplex algorithm to minimise the sum squared difference between the experimental singly-labelled peptide spectrum broadened by a convolution with Gaussian distributions of weak coupling regime Pake patterns and the experimental spectrum from the doubly-labelled peptides (note that the procedures adapted here are only valid if the dipole coupling does not exceed the hyperfine couplings). The Pake patterns were calculated with $J = 0$ (i.e. zero exchange) and such that the singularities all lie within the field range of interest. In total 3491 Pake patterns were formed with a dipolar splitting corresponding to distances between 0.51 and 4 nm (the 0.51 nm lower limit was chosen as an arbitrary limit where the assumption that $J = 0$ is certainly no longer valid). The routine furthermore allows the use of either one or two Gaussian distributions of Pake patterns for fitting. However, tests showed that allowing the use of a pair of Gaussian distributions for the convolution resulted in better fits (as expected) but a split distribution profile, regardless of the true nature of the broadening function. The mean distance and standard deviation were reproducible using either convolution method, consistent with the findings of Hustedt and co-workers [5]. The results shown in this paper employ the approach of fitting a monomodal Gaussian distribution only.

2.4. Elucidating the dipolar broadening function

In the previous section the dipolar broadened EPR spectrum was modelled as a convolution of the uncoupled line shape with a dipolar broadening function. However, it is also possible to directly derive the dipolar broadening function from the coupled and uncoupled spectra and consequently the distance and distance-distribution of simulated Pake patterns.

Rabenstein and Shin found the dipolar broadening function by deconvolving the coupled and non-coupled EPR spectra (d and s, respectively) in Fourier space and then transforming the function back to real space. This is shown by Eq. (6) where b is the broadening function, F and F^{-1} are the forward and inverse Fourier transforms, respectively.

$$b = F^{-1}[F(d)/F(s)] \tag{6}$$

The broadening function was analysed by assuming that it has the form of a strong coupling regime Pake pattern and applying a formula to find the average distance and variance [3].

Deconvolution is an unstable algorithm; it produces high amplitude components that obscure the line shape in both the time and, particularly, frequency domain due to the necessity of dividing by approximately zero. To increase the fidelity of the real space broadening function for analysis with the Rabenstein and Shin formulae, the deconvolved product may be cut to avoid the high frequency noise or fitted with up to two Gaussians which are then transformed back to the frequency domain [15,24]. Hubbell and co-workers have produced a low-noise broadening function by adding a slight bias (<0.01%) to all AC components of the Fourier transform of the non-coupled spectra (the denominator of the deconvolution equation) and by low-pass filtering of the broadening function itself [4]. This avoids division by near zero values. The Hubbell method differs from that of Shin; it uses a combination of deconvolution and convolution procedures to fit up to 50 weighted Pake patterns to the broadening function and simultaneously convolves them with the singly-labelled spectrum to produce a fit to the doubly-labelled protein spectrum.

The program "DipBF" was written using Matlab 7.0 to determine the dipolar broadening function from the CW EPR spectra. Two methods were used: a convolution matrix of the singly-labelled peptide spectrum and Fourier deconvolution.

2.5. Convolution matrix method

This technique uses the principle that the coupled spectrum, d, is a convolution of the uncoupled line shape, s, with a broadening function, b:

$$d = s \otimes b \tag{7}$$

Knowledge of the doubly labelled spectrum and the formation of the convolution matrix of *s*, *conv(s)* will yield *b* which is approximately related to the inter-spin distance-distribution, *D*, by the Pake patterns (modelled as being in the weak coupling regime), *p*:

$$b = p\ D \tag{8}$$

Also therefore note that, overall *D* and *d* are related by:

$$d = [p\ conv(s)]\ D \tag{9}$$

The *conv(s)* formed by DipBF is a square matrix (with dimensions equal to the number of data points collected in the CW experiment); edge effects (distortions of *b*) should be avoided by ensuring adequate baseline in both *s* and the matrix of Pake patterns (as used for convolution). To test for numerical stability of the deconvolution approach, the compact singular value decomposition (csvd) was made using the regularisation tools of Hansen as shown by Eq. (10), where *U* and *V* are the left and right singular vectors of *s* [25,26]. In this case the csvd corresponds to diagonalisation of the matrix.

$$conv(s) = U\ c\ V \tag{10}$$

A plot of log(*c*) (singular values) showed that *conv(s)* satisfies the discrete Picard condition, i.e. the singular values decay gradually to zero for the singly-labelled peptides and hence they do not have numerical rank; the broadening function cannot be found from least squares fitting of *d* by *conv(s)* and the problem is termed ill-posed. Similarly the singular values for *p* and [*p conv(s)*] were plotted and Eqs. (7)–(9) were found to be ill-posed (data not shown).

The maximum entropy method (MEM) has been used to solve the ill-posed problems [27]. MEM intrinsically suppresses the negative portions of the output (e.g. *b* in Eq. (7)). In EPR, MEM has been used previously for accurately determining distances and distance-distributions from double quantum coherence (DQC) EPR results (using the result from Tikhonov regularisation—another method of solving ill-posed problems—as a seed) [28]. MEM was used to find *D* by solving Eqs. (7) and (8) in the distance range 0.51–4 nm (physically realistic results were not produced by using MEM to solve Eq. (9)).

The reliability of the MEM method to find *D* was assessed by using test data sets generated by artificially broadening the experimental uncoupled spectrum (i.e. 4K(3)) with one or two Gaussian distributions of Pake patterns. In general the distance, standard deviation and distance profile were reproduced well for distances between 0.7 and 1.7 nm. Reproducing the profile breaks down for both shorter distances and mean distances above 1.7 nm, although the mean distance is reproduced approximately for distances up to 2.0 nm. If the presence of high levels of singly-labelled peptide as an impurity was assumed in these simulations, the output distances were longer than the input distances used in the simulation of the doubly-labelled peptide spectrum.

2.6. Fourier deconvolution

The principle of Fourier deconvolution for this problem is given by Eq. (6). The broadening function, *b*, found from deconvolution can then be implemented by DipBF to find the distance-distribution using the maximum entropy method to solve Eq. (8).

In DipBF the uncoupled, *s*, and coupled, *d*, spectra are fast Fourier transformed. The spectra are then divided with respect to one another (Eq. (6)) and the result is centred at zero time. A boxcar filter function is applied with a user-defined width (a window function width of 30 data points was found to be a good compromise between cutting the noise and allowing maximum signal to pass for the data discussed here) and the spectrum outside of the boxcar was zero-filled to the original number of data points. This cuts the high amplitude, high frequency noise which would otherwise obscure *b* and is essentially equivalent to low pass filtering. The imaginary part of the data was discarded since it is zero, as expected for properly deconvolved spectra.

Artefacts arising from the use of the boxcar function (sinc waveforms) and interference from noise affect the frequency domain spectrum obtained by transforming the deconvolved result. Fitting the broadening function in the time domain with a pair of Gaussians gives a pair of Gaussians in the frequency domain after back Fourier transformation, with no transformation artefacts. The transformed data was used to give the distance-distribution profile, *D*, using the MEM to solve Eq. (8).

Using example data it was found that for broad distributions the direct method and Gaussian fit method gave similar mean distances and standard deviations. Narrow distributions were best reproduced directly since the Gaussians in Fourier space did not give good fits to the transformed resolved Pake pattern. In general, the distance profiles obtained for these test cases by the two-step convolution matrix method were reproduced by the Fourier deconvolution techniques.

Rabenstein and Shin reported that monoradical impurities could be removed during analysis because they appear in the broadening function almost as a delta function at zero frequency [3]. Our own modelling has shown that this is only true for very short inter-spin distances which have distinct broadening functions compared to the delta function. Longer distances (greater than approximately 1 nm) require that any radical impurities are removed prior to signal processing to avoid obscuring the true profile.

2.7. DEER

The effect that the excitation bandwidth given by non-ideal pulses in the four-pulse DEER experiment has on the simulated spectrum was studied, starting from the theory developed for the corresponding three-pulse experiment by Tsvetkov et al. [29,30]. This theory assumes that

only the resonance offsets of the spins, and the secular part of the dipole–dipole Hamiltonian,

$$\widehat{H}_{\mathrm{sec}} = \omega_{dd}\widehat{S}_{Az}\widehat{S}_{Bz} \tag{11}$$

with the orientation- and distance-dependent dipole–dipole coupling ω_{dd}, need to be considered in the description of spin evolution and that observer pulses excite exclusively A spins and pump pulses excite exclusively B spins. During the rectangular pulses of finite length, both the static and the m.w. Hamiltonians are taken into account. Within these assumptions the theory suggests that finite pulse lengths and limited bandwidth result in two significant differences with respect to a description using ideal pulses. First, there is a decrease in modulation depth with increasing dipole–dipole coupling, and second, there is a time shift of the zero time of the dipolar oscillation by half the length of the initial observer $\pi/2$ pulse. The latter effect does not depend on the strength of the dipole–dipole coupling and can be easily accounted for in data analysis for the dead-time-free four-pulse DEER experiment, as the actual zero time coincides with the maximum of the signal trace.

The dependence of the modulation depth on pulse lengths and on the strength of the dipole–dipole coupling was studied for four-pulse DEER by numerical density operator computations using subroutines from the EasySpin library [31,32]. This way the remaining assumptions were relaxed. Specifically, we include the pseudo-secular part of the dipole–dipole Hamiltonian,

$$\widehat{H}_{p\mathrm{sec}} = -\frac{\omega_{dd}}{2}(\widehat{S}_{Ax}\widehat{S}_{Bx} + \widehat{S}_{Ay}\widehat{S}_{By}) \tag{12}$$

and assume that all m.w. pulses act on all spins in the system according to their resonance offsets from the frequency of the pulse. The only assumptions retained are that the resonance frequencies of the observer and pumped spins are uncorrelated, the pulses have rectangular shape, and the exchange coupling between the spins can be neglected. If the exchange coupling were known the last assumption could be relaxed. Likewise, orientation correlation of the spin labels could be easily introduced into the computations, if a model for the relative geometry were given.

The observer pulse frequency (local maximum of the nitroxide absorption spectrum near the low-field edge) and pump frequency (global maximum of the spectrum) are chosen as in the experiments. The resonance frequencies of the two coupled electron spins were varied independently throughout the nitroxide spectrum. For each pair of resonance offsets from the observer frequency the weighting is computed as the product of the intensities at the two resonance frequencies found from an experimental echo-detected EPR spectrum of the nitroxide radical. Computations were performed in a reference frame rotating at the observer frequency. During the pump pulse with length t_p, the Hamiltonian describing relative frame rotation,

$$\widehat{H}_{rot} = \Delta\omega_{mw}(\widehat{S}_{1,z} + \widehat{S}_{2,z}) \tag{13}$$

is subtracted, which corresponds to a slowdown of the frame rotation by angular frequency $\Delta\omega_{mw}$, so that the pump pulse is applied in a frame rotating with the pump frequency. The slower rotation is afterwards compensated for by applying only $\widehat{H}_{rot}$ for a time t_{p}. This treatment is possible since $\widehat{H}_{rot}$ commutes with all terms of the static Hamiltonian, including $\widehat{H}_{p\mathrm{sec}}$. The detection operator corresponds to quadrature detection on both spins. For detection, 13 points of the signal trace were summed with the time increment between these points being 4 ns and the 7th point coinciding with the echo maximum. This corresponds to the 48 ns integration window for the echo signal with 4 ns time resolution of the SpecJet digitizer used in the experiments.

In agreement with the theory of Tsvetkov et al. we find that for coupling strengths of the order of the excitation bandwidth and smaller, only the modulation depth depends on the coupling strength [29]. This approximation of moderate excitation bandwidth effects is valid down to modulation depths, λ, that are 1/10 of the maximum modulation depth λ_0, which is encountered in the limit of very small coupling ($\omega_{dd} \to 0$). For even larger couplings, the modulation phase and frequency are significantly affected. In this regime of strong excitation bandwidth effects, a correction is not promising, as the remaining modulation hardly exceeds the noise level within a reasonable measurement time and because a further error source is introduced by exchange couplings.

In the regime of moderate excitation bandwidth effects, simulations were performed for several typical sets of pulse parameters (Fig. 4). In general, the dependence of the modulation depth on ω_{dd} can be fitted quite satisfactorily by a Gaussian

$$\lambda = \lambda_0 \exp\left(-\frac{\omega_{dd}^2}{\sigma_{exc}^2}\right) \tag{14}$$

where σ_{exc} is the effective excitation bandwidth of the whole four-pulse DEER experiment. This effective excitation bandwidth is found to depend on the lengths of both the pump and observer pulses. For the pump pulse this is because a large bandwidth is required to invert both components of the dipolar doublet of the B spin and thus the local field at the A spin, as already remarked earlier [14]. However, such inversion also shifts the resonance frequency of the A spins by the dipolar coupling frequency (ω_{dd}). Hence, subsequent echo refocusing by the final observer pulse can only take place if this pulse can invert the shifted transitions. A significant shortening of the pump pulse while maintaining its flip angle π and the flip angles and lengths of the observer pulses thus results in a strong increase in the modulation depth, but only in a moderate improvement of the effective excitation bandwidth (compare Fig. 4A and B).

The values for λ_0 obtained by fitting the data for our standard pulse lengths are in good agreement with our

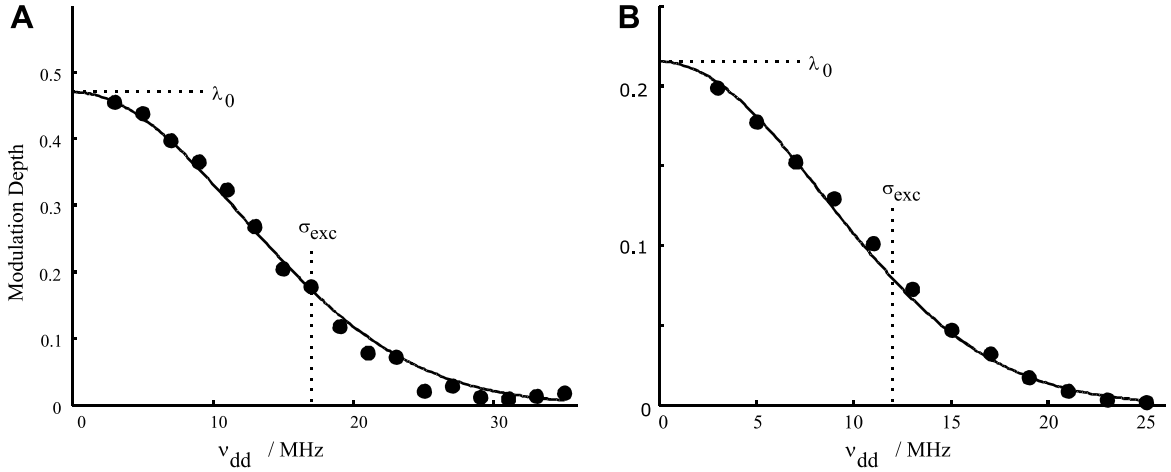

Fig. 4. Dependence of the modulation depth λ on the dipolar coupling frequency $\nu_{dd} = \omega_{dd}/2\pi$ in the four-pulse DEER experiment. Full circles correspond to numerical density operator simulations of the whole pulse sequence and solid lines to a Gaussian fit according to Eq. (14). The length of all observer pulses is 32 ns. (A) Pump pulse length $t_p = 12$ ns, effective excitation bandwidth $\sigma_{exc} = 17$ MHz. (B) $t_p = 32$ ns, $\sigma_{exc} = 12$ MHz.

experimental findings, indicating that the idealizing assumptions that remain in our approach are fulfilled. For data analysis in terms of distance-distributions, knowledge of λ_0 is not required, as the modulation after background correction is renormalized to unity amplitude. Excitation bandwidth correction thus only requires incorporation of the second factor on the right-hand side of Eq. (14) into the kernel, K, used in simulations of DEER time-domain data and in Tikhonov regularisation. The corrected kernel is given by:

$$K(t,r) = \int_0^1 \exp\left(-\frac{\omega_{dd}^2}{\sigma_{exc}^2}\right)\cos(\omega_{dd}t)d\cos\theta \qquad (15)$$

using the value of σ_{exc} obtained from the density operator computations for the experimental pulse lengths. This excitation bandwidth correction has been incorporated as an additional tool into DeerAnalysis2006 [12].

3. Experimental results and discussion

The secondary structure of the peptides was characterised by circular dichroism (CD) and nuclear magnetic resonance (NMR) methods [33,34]. The peptides were found to be essentially α-helical in a mixture of 1:1 (v/v) water and trifluorethanol (TFE) at room temperature but with considerable fraying at the termini. A spin-labelled peptide model was constructed assuming a perfect and rigid α-helix structure. Flexible spin labels were added to the cysteine residues and the trajectories of distances between the nitroxide moieties was monitored over 0.1–0.2 ns using an MM2 force field [35]. The mean distances and their standard deviations were used as guidelines for the approximate distances expected from the EPR experiments. The modelled distances for the 4K peptides ranged from 1.07 ± 0.31 nm for 4K(3,7) to 2.64 ± 0.55 nm for 4K(3,18) and was 4.61 ± 0.46 for 7K(3,32). In general, the distribution profiles were well approximated as Gaussian.

3.1. CW EPR

The CW EPR spectra of the peptides were recorded at 50 K in water/TFE frozen solutions. The distances and distance-distributions were obtained by the analysis techniques outlined in Section 2.[4] The results for the 4K peptides are given in Table 2 and Fig. 5. The CW spectra of 7K(3,32) in frozen solution were very similar to their 4K(3) analogues. In general the results follow the trend in distances given by the α-helical model. Additionally, each method for evaluating the distance indicates a break-down of the CW analysis techniques for the peptides with longer inter-spin distances such as 4K(3,12) and 4K(3,18), indicating the upper limit for these techniques. Detailed accounts of the results from each method are given below.

3.2. Second moment

The results show that there is a good correlation between the distance from the second moment calculation and the α-helix MM2 modelled distance trend for 4K(3,7), 4K(4,11), 4K(3,11) and 4K(3,14), although the statistical errors for 4K(3,11) and 4K(3,14) are not negligible, presumably because they are near the upper limit of the applicable region for this type of analysis. The second moment distances for 4K(3,13), 4K(3,12) and 4K(3,18) are dubious; the latter two do not have positive second moment differences with

[4] We also attempted the use of the ratio of peak heights (d_1/d) method [36], despite showing the same trend as the other techniques the ratios did not lead to realistic distances. This is probably due to the need for well-defined inter-spin distances, a condition the peptides are not expected to fulfil.

Table 2
Results from the second moment analysis, convolution of dipolar coupling patterns with the uncoupled spectrum (DipCon), convolution matrix method and direct Fourier deconvolution compared to the results from the α-helical model calculations for the 4K peptides (more details may be found in the text and the graphical results are shown in Fig. 5)

Peptide		α-Helical model		Second moment		DipCon (monomodal)			DipBF: convolution matrix		DipBF: Fourier deconvolution		
		$\bar{r}$/nm	$\sigma_{\langle r\rangle}$/nm	$\bar{r}$/nm	±Er/nm	$\bar{r}$/nm	$\sigma_{\langle r\rangle}$/nm	$\sigma_{fit}/10^{-5}$	$\bar{r}$/nm	$\sigma_{\langle r\rangle}$/nm	$\bar{r}$/nm	$\sigma_{\langle r\rangle}$/ nm	$\sigma_{MEM}/10^{-4}$
4K(3, 7)	MTS	1.07	0.31	1.07	0.07	1.14	0.29	4.70	1.17	0.36	1.14	0.39	1.3
	SAT			1.02	0.05	1.28	0.35	5.69	1.16	0.42	1.14	0.46	1.6
4K(4, 11)	MTS	1.20	0.40	1.09	0.09	1.26	0.38	4.20	1.30	0.43	1.28	0.44	1.7
	SAT			1.13	0.04	1.33	0.37	2.99	1.36	0.37	1.36	0.39	1.3
4K(3,11)	MTS	1.70	0.43	1.32	0.23	1.46	0.38	3.67	1.50	0.38	1.47	0.33	2.4
	SAT			1.43	0.18	1.77	0.49	2.74	1.60	0.38	1.58	0.33	3.6
4K(3,14)	MTS	1.89	0.48	1.50	0.47	1.84	0.47	3.05	1.68	0.39	1.65	0.34	6.2
	SAT			1.53	0.3	1.79	0.37	2.18	1.65	0.38	1.61	0.31	4.8
4K(3,13)	MTS	2.03	0.53	1.68	1.06	1.66	0.00	2.09	1.70	0.39	1.61	0.33	4.9
	SAT			1.76	0.62	1.76	0.01	2.36	1.71	0.39	1.66	0.34	6.7
4K(3,12)	MTS	2.22	0.29	N/A	N/A	1.95	0.02	2.25	1.79	0.40	1.65	0.33	6.9
	SAT			1.78	0.62	2.07	0.00	2.23	1.77	0.40	1.68	0.34	8.3
4K(3,18)	MTS	2.64	0.55	1.73	1.28	2.02	0.02	2.65	1.81	0.40	1.66	0.33	8.0
	SAT			N/A	N/A	—	—	—	1.94	0.43	1.70	0.34	11

$\bar{r}$ is the mean distance, $\sigma_{\langle r\rangle}$ is the standard deviation in the distance result, ±Er for the second moment analysis represents the error produced by the polynomial baseline correction applied to the experimental data, σ_{fit} is the standard deviation between the best fit artificially broadened uncoupled spectrum (from the 4K(3) peptide) and the experimental doubly-labelled peptide spectrum, σ_{MEM} is the maximum entropy method regularisation parameter, N/A indicates that the second moment result was negative for the peptide.

respect to 4K(3) or 7K(3,32) and all three peptides have extremely large statistical errors. The second moment analysis may give artificially short distances if the majority of the high end of the distance-distribution cannot be resolved in the EPR spectrum (no distance results above 1.78 nm are returned by this method). Such an error cannot be recognised without comparison to results obtained using a different data analysis procedure, due to the fact that this method does not reveal a distance-distribution. The biased distance results may be the reason why only the distance for 4K(3, 7) corresponds well with the actual value from the α-helix model, as it is the only peptide which is predicted, from the MM2 calculations, not to have a significant distance population above 1.5 nm.

3.3. DipCon

By following the same distance trend as the modelled structures (for peptides modelled as having inter-spin distances less than 1.9 nm) the DipCon results in Table 2 and Fig. 5B indicate that the frozen peptides do form α-helices. Additionally there is good overlap between the model and the results for the standard deviation on the distance results (Table 2). The distributions are very narrow for 4K(3, 12), 4K(3, 13) and 4K(3, 18)-MTS and no distance can be found from the 4K(3, 18)-SAT data. Such anomalous results indicate a failure of the convolution method for elucidating distances for these peptides and hence these results should be discounted.

Deviations from the expected distances were seen for 4K(3, 7)-SAT, where the DipCon result was larger than expected from the model, and 4K(3, 11)-MTS, where the DipCon distance was shorter. In the case of 4K(3, 11)-MTS the spectrum is broader for the MTS label than the SAT version (not shown) and hence the deviation of the result from the model appears to be a genuine effect. Except for the 4K(3, 14) results the DipCon distances indicate that the MTS-labelled peptides have a shorter inter-spin distance than the SAT-labelled versions although no conclusions as to why can be drawn using the available data. The fitting was poor for 4K(3, 7) (particularly the SAT-labelled peptide) although the actual distances and standard deviation results are in line with those predicted by the model. The poor fitting is likely to be due to significant exchange coupling which causes spectral narrowing. In fact, for couplings that are of the same order of magnitude as the width of the nitroxide spectrum (about 180 MHz), the assumption of a uniform coupling pattern for all spin pairs in the sample is no longer fulfilled. This is because the coupling pattern then depends on the ratio between the combined dipolar and exchange coupling to the difference of the resonance frequencies of the two spins in the absence of the coupling. The slight distance increase between spin labels (in the order of 0.1 nm) due to an extra turn of the α-helix for 4K(4, 11) compared to 4K(3, 7) appears to be sufficient to allow for good fits to be obtained and hence the distance results are more reliable.

3.4. DipBF: Convolution matrix

The MEM regularisation values, σ_{MEM}, used for the MEM were 3×10^{-5} and 1×10^{-4} for the first and second

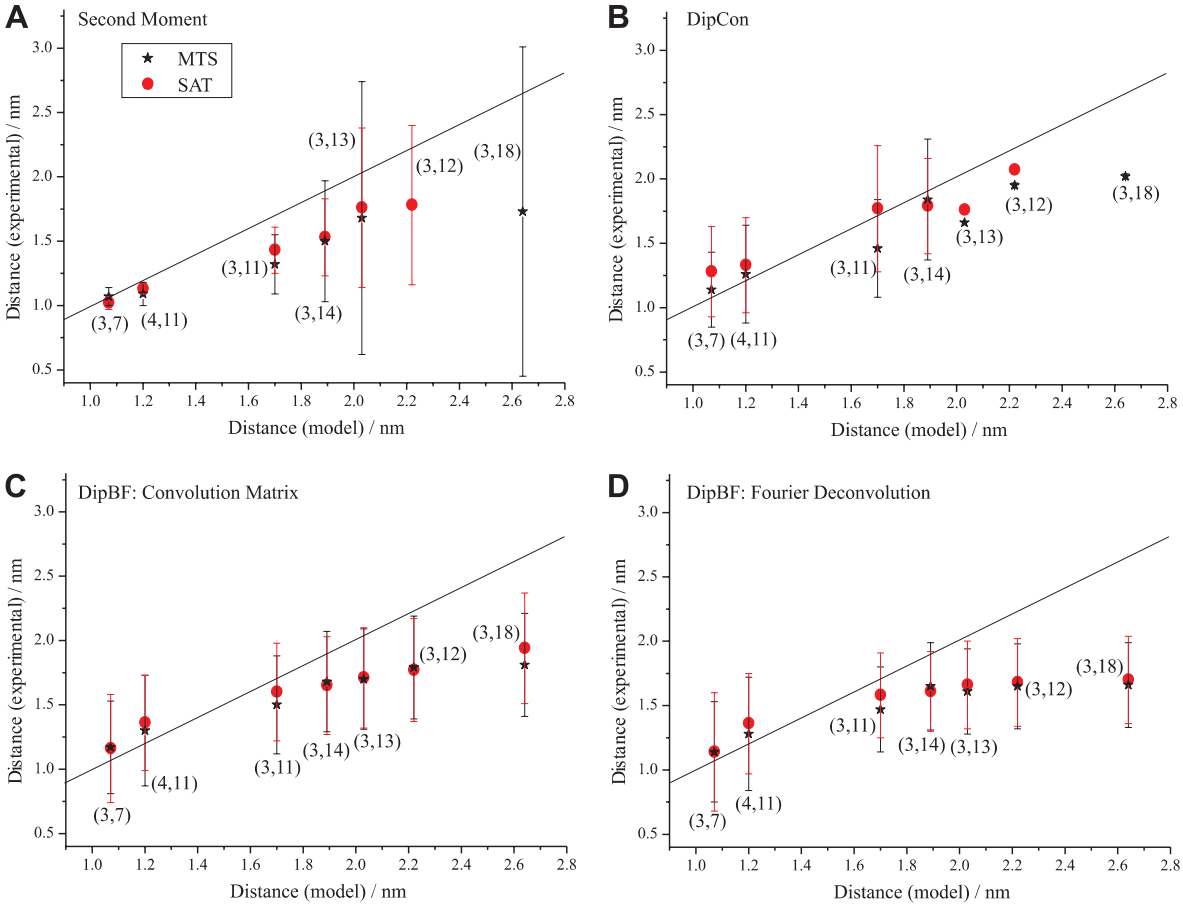

Fig. 5. Graphs showing the results given in Table 2 for the MTS (black) and SAT (red)-labelled peptides. The mean distance results and either the standard deviation in the spread or (in the second moment analysis case) the associated error are plotted against the mean results (the standard deviation has been omitted for clarity but these may be found in Table 2) from the α-helical model calculations: (A) second moment analysis; (B) convolution of dipolar coupling patterns with the uncoupled spectrum (computer program name: DipCon); (C) convolution matrix method (computer program name: DipBF); (D) Fourier deconvolution (computer program name: DipBF). The results are marked by the positions of the labelled cysteine residues.

step respectively (i.e. solving Eqs. (7) and (8)). Assuming that the α-helix is the dominant conformation, the two-step convolution method provides reasonable results up to approximately 1.7 nm (Fig. 5). For peptides with a predicted mean distance between spin labels greater than this value a non-zero baseline is given in the distribution profile (not shown) at the maximum cut-off point of 4 nm. Hence, unlike the DipCon method which indicates a failure by producing very narrow distributions, the DipBF: Convolution Matrix method in this situation produces a non-zero baseline at long distances. 4K(3,11), 4K(3,13) and 4K(3,14) failed less severely than 4K(3,12) and 4K(3,18) indicating that the distance and standard deviation results for these peptides are more accurate and that the Convolution Matrix method completely fails only for actual inter-spin distances greater than 2.0 nm.

The distribution profiles for the 4K(3,7) and 4K(4,11)-MTS peptides are bimodal in nature. This may be a true result but it could be a side-effect of the maximum entropy technique because the distributions are constrained to begin at 0.51 nm. If the bimodality is indeed due to this constraint then these three peptides probably have an inter-spin distance population at shorter distances than those which can be accounted for by DipBF. However, tests with simulated data indicate that the mean and standard deviation are still well reproduced for this situation.

3.5. DipBF: Fourier deconvolution

The data reported in Table 2 and shown in Fig. 5D are based on direct Fourier deconvolution rather than Gaussian fits of the deconvolved data. For short distances the only effect of using the direct method is to lose the more physically realistic smoothness of the distance profiles. This is because the Pake patterns are fitted to the dipolar broadening function and the sinc waveform artefacts arising from Fourier transformation of the boxcar filter function. The simulations discussed in Section 2 above indicate that distances longer than approximately 1.3 nm are more accurately reproduced with this direct method. Assuming that the principle conformation of the 4K peptides is α-helical, distances up to approximately 1.6 nm (4K(3,7), 4K(4,11) and 4K(3,11)) can be measured with accurate standard deviations using the Fourier deconvolution method. Above

the 1.6 nm threshold, little trend can be seen in the mean distance results except that 4K(3,18) appears to have the largest inter-spin separation.

Table 2 gives the sigma value, σ_{MEM}, for MEM regularisation. Whereas for the two-step convolution matrix method the two regularisation parameters did not need to be changed across the peptide series, for Fourier deconvolution the regularisation parameter appears to be indicative of the accuracy of the result. Comparing σ_{MEM} values to the peptide model results shows that a value below 3×10^{-4} corresponds to accurate mean and standard deviation results, while values above 5×10^{-4} imply that the analysis has failed and that the dipolar coupling is too weak to be resolved by analysis of the CW EPR spectrum. As for the two-step convolution matrix method, failed cases also resulted in a non-zero distance baseline in the distance-distribution at longer distances although this was less pronounced.

The Fourier deconvolution method can offer more insight into the apparent multimodal distributions at short distances given by both DipBF methods by comparing the dipolar broadening patterns from the experimental cases with those from models. There are three possibilities for the multimodal distributions obtained for 4K(3,7) and 4K(4,11):

(a) The presence of a singly-spin-labelled peptide impurity which gives an underlying signal in Fourier space and thus obscures the broadening function. This would cause a splitting of the distribution profile and an increase in the mean distance measurements, however, this is unlikely based on the purity assessment of the mass-spectrometry and HPLC results.
(b) Limitations of the regularisation method. Split distributions were seen to be a particular problem for inter-spin distances with significant population below 0.51 nm.
(c) True bimodal distribution due to either the peptide or spin label conformation.

Each of these situations was modelled and the broadening functions in real and Fourier space compared to those from the 4K peptides. Only case (c) fitted the criteria shown experimentally, by having a two-tier broadening function in both real and Fourier space. The conclusion was drawn that 4K(3,7) and 4K(4,11) have two distinct sets of distances in their frozen state which are not populated equally for SAT and MTS. There was no evidence from the CW EPR data to suggest that the other spin-labelled peptides have bimodal distributions. The MM2 models did show that for rigid α-helices some spin-labelled peptides did give a bimodal inter-spin distance-distribution. For example 4K(4,11) had a bimodal distribution due to interference from the long side chains of the lysine residues at positions 5 and 10 restricting the trajectory of the spin labels attached to cysteines 4 and 11.

3.6. DEER

Using the DEER signal from the singly-labelled peptide, the actual form of the background function was found to be homogeneous ($\exp[-kt^{D/3}]$) with a fractal dimension D of 3.77 and 3.78 for MTS and SAT peptides, respectively. The appearance of a fractal dimension larger than three is not well understood. It corresponds to an underrepresentation of short distances compared to a homogeneous distribution in three dimensions ($D=3$) and it would be expected for objects which repel each other. However, as the background function for the singly-labelled peptide is reproducible, this value could be incorporated into DeerAnalysis 2006 for the deconvolution of V_{intra} from V_{inter} (where V are the signal intensities due to long range, intra-molecular, and short range, inter-molecular, dipolar couplings, respectively) to give just the DEER time-domain signal due to directly dipolar coupled spins [12].

Fig. 6 shows the modulation depths for the signals from the MTS-labelled peptide. It illustrates that as the expected distance between the spin labels increases (see Table 3) the modulation depth increases for the 4K peptides. 4K(3,18) has a very similar modulation depth to 4K(3,32)-MTS because both exhibit distances which can be measured well by the DEER experiment.

The distances and their distributions were found from the time traces using the L-curve method of Tikhonov regularisation with determination of the optimum regularisation parameter from the L-curve in DeerAnalysis 2006. The results are given in Table 3 and Fig. 7 for the idealised kernel function and the kernel function with excitation bandwidth correction. The distances found for the 7K peptide are shorter than modelled and exhibit a broader distribution. This most probably indicates that the peptide does not adopt a perfectly rigid α-helical conformation, but has some backbone flexibility. For the closely spaced residues in the 4K peptides the influence of this flexibility on the distance-distribution is presumably within experimental error.

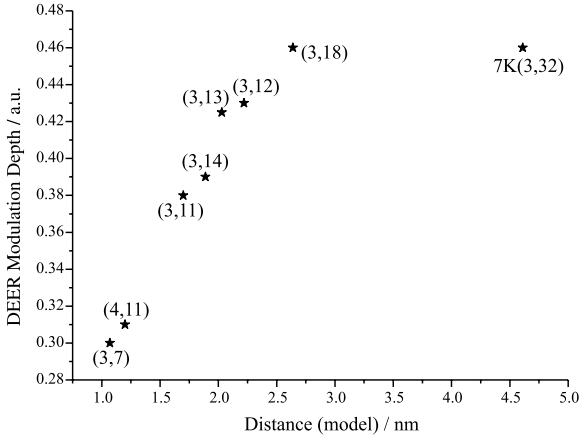

Fig. 6. Modulation depth values from the background corrected MTS-labelled peptide DEER signals.

Table 3
The average distance and the standard deviation for the peptides given by Tikhonov regularisation using DeerAnalysis2006, compared to the α-helical model results

Peptide		α-helical model		Idealised Tikhonov reg.		Excitation bandwidth corrected Tikhonov reg.	
		$\bar{r}$/nm	$\sigma_{\langle r\rangle}$/nm	$\bar{r}$/nm	$\sigma_{\langle r\rangle}$/nm	$\bar{r}$/nm	$\sigma_{\langle r\rangle}$/nm
4K(3,7)	MTS	1.07	0.31	1.94	0.37	1.60	0.40
	SAT			1.93	0.35	1.83	0.24
4K(4,11)	MTS	1.20	0.40	1.79	0.20	1.65	0.15
	SAT			1.87	0.31	1.51	0.35
4K(3,11)	MTS	1.70	0.43	1.88	0.30	1.58	0.36
	SAT			2.02	0.26	1.88	0.32
4K(3,14)	MTS	1.89	0.48	2.21	0.39	2.10	0.41
	SAT			2.15	0.34	2.01	0.39
4K(3,13)	MTS	2.03	0.53	2.02	0.30	1.92	0.28
	SAT			2.14	0.33	2.00	0.38
4K(3,12)	MTS	2.22	0.29	2.10	0.26	2.03	0.24
	SAT			2.23	0.29	2.15	0.31
4K(3,18)	MTS	2.64	0.55	2.42	0.44	2.32	0.49
	SAT			2.63	0.47	2.58	0.49
7K(3,32)	MTS	4.61	0.46	4.17	0.60	4.16	0.61
	SAT			4.39	0.64	4.31	0.82

Idealised Tikhonov and excitation bandwidth corrected Tikhonov refer to the kernel function used in the calculation, see text for further details.

However, we cannot safely exclude that the broadening of the distribution is caused by insufficient background correction.

The correction to the kernel consistently leads to a shorter average distance result for the 4K peptides, but not by a constant amount across the series. The corrected distances and standard deviations are roughly in line with those expected from the MM2 simulation of a 4K α-helix for all but the shortest distances (i.e. the 4K(3,7) and 4K(4,11) peptides).

Correction of the kernel function also reduces the distance for the 7K(3,32)-SAT data. Additionally, unlike for the other corrected data, the standard deviation also changes significantly upon the kernel change. However, inspection of the distance profiles (not shown) reveals that the effect is entirely due to a small artefact at short distances (1 nm) which increases upon excitation bandwidth correction. The artefact is likely to be caused by random noise in the experimental spectrum; suppressing the artefact does not appreciably affect the simulated time-domain data and there is no reason to expect a true distance result in this region. The case of 7K(3,32) highlights two important points; firstly, that taking the average distance and standard deviation over the whole distance range (1–8 nm) may lead to contributions from artefacts which have no physical relevance, and secondly that using the excitation bandwidth correction may lead to a higher weighting of artefacts if these appear at short distances. For systems with significant contributions only at distances above 2 nm, which do not explicitly require consideration of the excitation bandwidth limitations, it is appropriate to refrain from such correction. This has the added benefit of considerably increasing the speed of computation.

The shortest distances, as expected for 4K(3,7) and 4K(4,11), do not seem to be recovered by the DEER experiment, even when the limited excitation bandwidth is taken into account. The molecular dynamics and the CW work imply that the DEER results are incorrect for these samples, and the probable source of the error is revealed by the numerical density operator computations which indicate that at distances below 1.3 nm, the zero time position becomes dependent upon the magnitude of ω_{dd} and the oscillation frequency no longer follows the standard theory. It is also likely that the exchange interaction is becoming comparable to the dipolar coupling (intermediate coupling regime) and this will increase the modulation frequency and therefore give a spuriously long distance [10]. The excitation bandwidth correction was found to be most useful for the peptides with an expected (modelled) average inter-nitroxide distance of about 1.7 nm and for larger distances where there is significant (within the standard deviation) distance population below approximately 2 nm.

3.7. Comparing the CW and DEER results

Table 2 and Fig. 5 compare the distance results for the 4K peptides given by convolution with a single Gaussian, the two-step convolution matrix method and Fourier deconvolution. The table shows that the three methods all give very similar trends and results, particularly for the shorter distances in 4K(3,7) and 4K(4,11). There is some discrepancy for 4K(3,7)-SAT between the Gaussian convolution method and the methods using the dipolar coupling broadening function. This is presumably due to the Gaussian distribution approximation being insufficient for 4K(3,7)-SAT. The analysis methods consistently fail

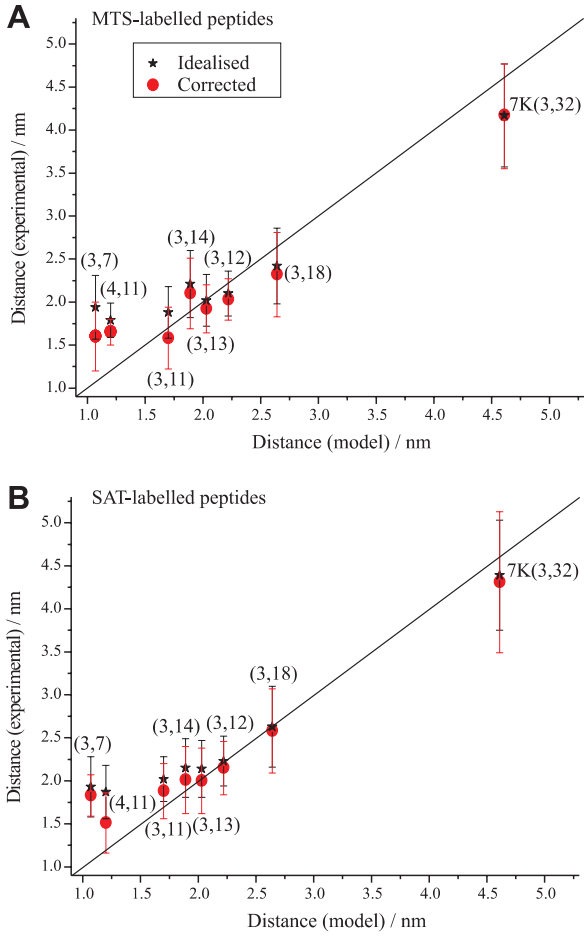

Fig. 7. Average distance and its standard deviation between nitroxide labels of the peptides as measured by DEER (using the L-curve Tikhonov Regularisation analysis method) compared to the results from MM2 calculations for rigid α-helices. The idealised results use the standard dipolar time domain kernel whereas corrected data take account of the limited excitation bandwidth of the pulse sequence: (A) MTS-labelled peptides; (B) SAT-labelled peptides. The model distance refers to the average distance between spin labels found from molecular dynamics simulations. The results are marked by the positions of the labelled cysteine residues.

for the longer distances; for the peptides this corresponds to 4K(3, 12), 4K(3, 13) and 4K(3, 18). The techniques display different characteristics for these long distances: the second moment method gives large statistical errors (greater than 1 nm) or negative results (marked as N/A in Table 2), the Gaussian convolution method gives a very narrow, unfeasible distribution for the longer distances (and does not produce a result at all for 4K(3, 18)-SAT) whereas the Convolution Matrix and Fourier Deconvolution methods have a non-zero baseline in the distance-distribution plots even at 4 nm. From the α-helix model the expected inter-nitroxide distances for these three peptides are above 2 nm. This would not be the case if the peptides were to have significant 3_{10}-helical content or if they were random coil (for example, in the case of a 3_{10}-helix the 4K(3, 12) peptide would have a mean inter-spin separation of 1.9 nm from MM2 calculations). The CW results therefore imply that the 4K peptides are predominantly α-helical, in agreement with the CD and NMR results.

The Gaussian convolution method results are compared to the DEER results in Fig. 8. The figure does not show the cases where the CW analysis did not lead to a realistic distribution of distances (namely 4K(3, 12), 4K(3, 13) and 4K(3, 18)). However, it shows all the DEER results from the 4K peptides since there is not a simple diagnostic test to disprove their validity except to compare to expected (modelled) values and those given by CW EPR studies. The average distances found from DEER and CW measurements most closely matched for 4K(3, 11), although there is also good agreement for 4K(3, 14) and 4K(4, 11)-SAT. The figure shows that the upper cut-off for reliable CW measurements and the lower cut-off for reliable DEER measurements for broadly-distributed distances between nitroxide spin labels are coincident at approximately 1.6 nm. This suggests that the techniques should be used in combination when distances between 1.2 and 2.0 nm are expected and accurate values are required. The widths of the distributions do not match so well, even for

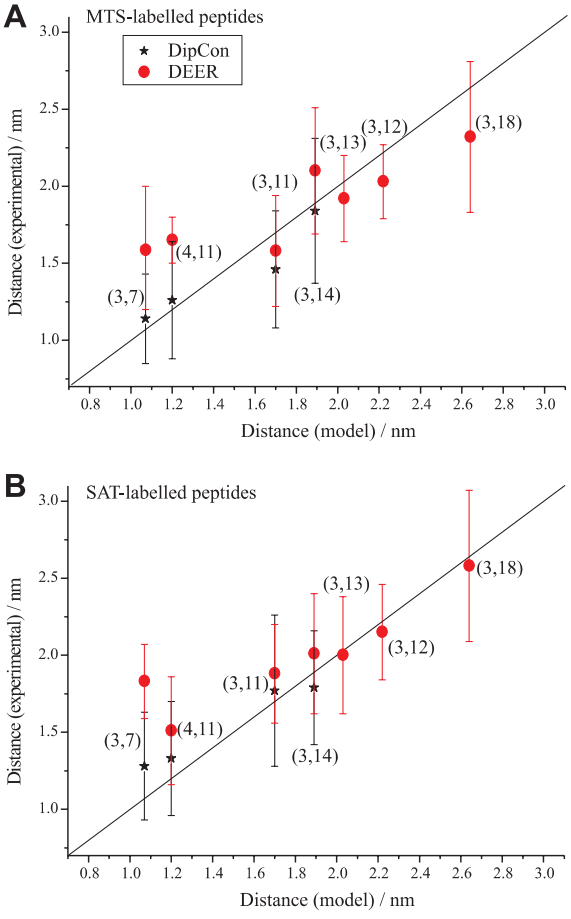

Fig. 8. Average distance and standard deviation results from Gaussian convolution (DipCon; no results are shown if the standard deviation was very small, see text for details) and excitation bandwidth corrected DEER: (A) MTS label; (B) SAT label. The model distance refers to the average distance between spin labels found from molecular dynamics simulations. The results are marked by the positions of the labelled cysteine residues.

4K(3,11), probably caused by an insufficient and dissimilar distance range for the CW and DEER analyses (lower limit of 0.5 and 1 nm, respectively). The DEER results for the 4K peptides (apart from the 4K(3,7) and 4K(4,11)) fit the α-helix model for the peptide well (Fig. 8). 4K(3,12) appears to have a narrow distribution compared to the other peptides, this was predicted by the MM2 simulations for an α-helix structure, compared to a 3_{10}-helix, because of the spin labels being at opposite sides of the peptide rod and thus the extremes of the normal distribution are disfavoured (the spin label cannot lie along the peptide backbone due to steric hindrance). There are some discrepancies between the DEER results and the perfect α-helical model, for example 4K(3,18)-MTS: they may be due to some backbone flexibility, kinks in the conformation of the peptide, fraying at the ends (particularly in the case of 4K(3,18) which has spin labels close to both the N- and C-termini), the way the spin labels orientate themselves, or insufficient computer modelling.

4. Conclusions

In this work a family of peptides were synthesised and spin-labelled in order to investigate and compare distance measurements using EPR. In particular, an upper distance limit for CW measurements of protonated spin labels and a lower bound for DEER measurements were found. A variety of methods such as CD, NMR and computer modelling (MM2 and CHARMM calculations) were used to analyse the conformation of the peptides, with and without nitroxide spin labels. Each of these methods produced results that were fully compatible only with the conclusion that the 4K peptides are α-helical in a solution of water/TFE but that the conformation is not rigid. The 7K peptide also seemed to be α-helical but, in contrast to the 4K peptides, the DEER results gave a significantly shorter mean distance and broader distribution than expected for a completely rigid helix.

The DEER results presented provided impetus to improve DEER methodology for measurements close to the lower boundary of applicability of this technique. The limit was found by density operator computations to depend on the lengths of both the pump and observer pulses as well as their separation and the effect was calculated using the density operator formalism. For the broad distribution of distances often encountered with spin labels, the lower cut-off has been found to be around 1.6 nm, even if the effect of excitation bandwidth limitations on the signal is accounted for. Significantly, even shorter distances were experimentally found to give DEER modulations with spurious frequencies that were lower than expected and thus correspond to longer distances than were probably present in the distributions. Double-quantum coherence (DQC) EPR spectroscopy may be useful for these shorter distances, see Ref. [37] for a detailed review of the topic. The excitation bandwidth correction often makes only a minor difference to the mean distance result from the analysis of the DEER spectrum but should be applied to data where the inter-spin population is expected to be significant at distances less than 2.0 nm. The excitation bandwidth correction has also been applied for the analysis of the DEER spectra given by spin labels attached to gold particles and has been incorporated into DeerAnalysis 2006 [12].

The peptides with saturated (SAT) and unsaturated (MTS) methanethiosulfonate spin labels did not give identical EPR results although all results implied an α-helical peptide [33]. Notably, the CW and DEER measurements led to the consistent conclusion that 4K(3,11)-MTS has a shorter inter-spin distance than 4K(3,11)-SAT and typically the SAT inter-spin distances appeared somewhat shorter than for the MTS-labelled peptides, particularly when the DipCon method of analysis was applied to the CW EPR data.

The CW and pulse EPR results obtained with this family of doubly-labelled peptides show conclusively that, with current technology, accurate inter-nitroxide distances in the range of 1.2–2.0 nm can be obtained in the presence of a conformational distribution of the spin labels only if CW and DEER methods are combined. Using a doubly-spin-labelled set of peptides based on a repeating sequence of $(AAAK)_nA$, we showed that the upper distance for elucidating accurate distances from CW data is in the region of 1.5–1.7 nm which is significantly shorter than previously found by Rabenstein and Shin using end-capped versions of the peptides and their method of Fourier deconvolution. The cut-off seemed to depend on the method of analysis used. Methods for finding the distribution of distances from CW data were comprehensively reviewed and further developed. It was shown that a combination of a variety of data analysis methods may give a more complete picture of a system but that contributions due to electron exchange and the general problem of resolution for an inhomogeneously-broadened line can still lead to large inaccuracies in the distance-distribution profile obtained. However, despite major overlap in the wide distribution profiles of the peptides the mean distances could be discerned through the combined use of CW and DEER techniques and thus the peptides could be distinguished.

5. Experimental

5.1. Peptide synthesis and spin labelling

The solid phase peptide synthesis (SPPS) was carried out using Fmoc protection of the N-terminus of the amino acids and orthogonal protecting groups for the side chains of the lysines and cysteines (t-boc and trt, respectively). The protected amino acids were purchased from Fluka. The resin, Fmoc-L-ala-PEG-PS, which had the first amino acid attached to the polyethylene glycol polystyrene support, was purchased from Applied Biosystems and the activators were from Novabiochem. A combination of HBTU and HOBt were used as the coupling reagents for lysine and

cysteine. To increase the yield of final peptide, each alanine residue was coupled twice. The first reaction used HBTU and HOBt and the second used PyBOP and HOBt. After the final deprotection the resin was washed with DCM and Methanol and left to dry under vacuum for 24 h. A mixture of 92% TFE (Sigma), 3% Phenol (Fluka), 3% EDT (Fluka) and 2% TES (Aldrich) was added to the dried resin in a separating column. The resin and cleavage mixture were left mixing for five hours before the solution was collected. The resin was washed with TFA (Applied Biosystems) and the run-off was added to the cleavage solution. Nitrogen was used to reduce the volume to less than 1 ml by blowing over the solution in a fume-hood. Diethyl ether was added and a precipitate was formed. The suspension was centrifuged and the solution removed. Two further aliquots of di-ethyl ether were added to the precipitate and centrifuged. The white solid was dried with a stream of nitrogen. The dry solid (the crude peptide) was dissolved in a mixture of water and TFE and lyophilised. This crude peptide was stored in the freezer. The peptides were purified using reverse phase high performance liquid chromatography, HPLC (Varian) employing a Phenomenex C18 semi-prep column. After lyophilisation the peptides were analysed by mass spectrometry which confirmed the pure product.

The nitroxide spin label (Toronto Research Chemicals) was dissolved in ethanol into a saturated solution. A five times molar excess of the label was added to the peptide in water. The label was found to react efficiently at room temperature in half an hour. The excess spin label, singly-labelled species and sulfinic acid were then separated from the doubly-labelled peptide using HPLC. The collected peptide fractions were lyophilised and then analysed using mass spectrometry. The results showed that there was no singly-labelled peptide impurity present in the double-cysteine peptides and also that the amount of unlabelled peptide was very small, if present at all. Multiple ionisations were common but the masses agreed well with the predicted values of 1940, 3392 and 2157 AMU for MTS-labelled 4K(3), 7K(3,32) and the 4K double cysteine peptides, respectively. The results for SAT-labelled peptides were correspondingly 2 or 4 AMU larger for singly- and doubly-labelled peptides.

5.2. Circular dichroism

Far-uv CD measurements were performed at room temperature and 4 °C with a Jasco J720 spectropolarimeter. The peptides were measured with and without spin labels and in varying amounts of trifluoroethanol from 0 to 50% by volume. The ellipticity was monitored for signs of helical structural motifs characterised by negative bands at 222 nm and 208 nm. The CD spectra showed an isodichroic point at 202 nm and maximum helical structure was given with 40% TFE which led to the conclusion that helices were formed but that they were in equilibrium with the random coil [38,39]. The ratio of the bands at 222 nm and 208 nm was close to unity which is indicative of an α-helix [40]. The effect of lowering the temperature was to increase the CD bands indicative of helix formation.

5.3. Nuclear magnetic resonance

NMR experiments were carried out on a Varian Unity INOVA 600 spectrometer operating at a ^{1}H frequency of 599.8 MHz. The probe was a 5 mm $^{1}H\{^{13}C, ^{15}N\}$ triple resonance type with a z-axis pulsed field gradient coil (with a gradient strength of up to 60 G cm^{-1}). Chemical shift values for the amino acids in the peptides were assigned using a combination of total correlation spectroscopy (TOCSY, 80 ms mixing time employing an MLEV17c isotropic mixing sequence) and nuclear Overhauser spectroscopy (NOESY, 150 ms mixing period). All experiments were run at 4 °C in water/deuterated TFE (50/50 v/v) at a peptide concentration of approximately 5 mM. The peptides were not nitroxide spin-labelled. The chemical shifts were interpreted using the method of Wishart and co-workers and were indicative of helical secondary structure motifs, particularly away from the termini [41]. The NOEs were classified as weak, medium or strong and these were used as constraints in CHARMM calculations which gave peptide structures based on α-helices [42,43].

5.4. CW EPR

Measurements were taken at 50 K with a Bruker E680 spectrometer operating at X-band and Oxford Instruments variable temperature unit. Peptide solutions were 0.1 mM and in 1:1 water and TFE. Hundred averages were taken with 8 μW power, 0.2 mT peak-to-peak modulation amplitude, 30 mT scan width and 2048 data points.

5.5. DEER experiments

The X-band spectrometer was a Bruker E580 with a variable temperature unit. The measurements were done with a Bruker 3 mm split ring EPR resonator, ER 4118X_MS3. The second microwave frequency was provided by a YIG oscillator (Magnetech Avantek AV78012). The peptide concentration was 0.1 mM in equivolume water/TFE. The pulse sequence is shown in Fig. 1. The experiment was run at 50 K. 4K(3, 18) and 7K(3, 32) were measured with a τ_2 of 3 μs, the 4K(3,7) sequence had a τ_2 of 1 μs, all other peptides were measured with a τ_2 of 2 μs. Prior to data analysis the time domain signal was phase corrected, this accounts for small phase errors made when setting up the DEER experiment as well as Bloch–Siegert shifts, as reported in Ref. [44].

5.6. Calculations

MM2 calculations were carried out using Chem3D Pro Version 10 [35]. The peptide backbones were made inflexible and only the nitroxide spin labels, cysteine side chains

and any close lysine side chains were able to move in the vacuum (other parameters included a 2 fs step interval, 10 fs frame interval, between 10,000 and 20,000 iterations, a heating/cooling rate of 1 kcal/atom/ps and a target temperature of 300 K). DeerAnalysis 2006 and all CW EPR analysis programs were written using Matlab 7.0.

Acknowledgments

The authors thank and acknowledge the assistance of Mr. Christian Bauer, Dr. Dahlia Fischer and Professor Heinz-Jürgen Steinhoff. J.E.B. and C.R.T. thank EPSRC for financial support. C.R.T. thanks the Royal Society for a University Research Fellowship.

References

[1] L.J. Berliner, S.S. Eaton, G.R. Eaton (Eds.), Distance Measurements in Biological Systems by EPR, KA/PP, 2000.
[2] H.-J. Steinhoff, N. Radzwill, W. Thevis, V. Lenz, D. Brandenburg, A. Antson, G. Dodson, A. Wollmer, Determination of interspin distances between spin labels attached to insulin: comparison of electron paramagnetic resonance data with the X-ray structure, Biophys. J. 73 (1997) 3287–3298.
[3] M.D. Rabenstein, Y.-K. Shin, Determination of the distance between two spin labels attached to a macromolecule, Proc. Natl. Acad. Sci. USA 92 (1995) 8239–8243.
[4] C. Altenbach, K.-J. Oh, R. Trabanino, J.K. Hideg, W.L. Hubbell, Estimation of inter-residue distances in spin labeled proteins and physiological temperatures: experimental strategies and practical limitations, Biochemistry 40 (2001) 15471–15482.
[5] E.J. Hustedt, R.A. Stein, L. Sethaphong, S. Brandon, Z. Zhou, S.C. DeSensi, Dipolar coupling between nitroxide spin labels: the development and application of a Tether-in-a-cone model, Biophys. J. 90 (2006) 340–356.
[6] M. Pannier, S. Veit, A. Godt, G. Jeschke, H.W. Spiess, Dead-time free measurement of dipole–dipole interactions between electron spins, J. Magn. Reson. 142 (2000) 331–340.
[7] A.D. Milov, K.M. Salikhov, M.D. Shirov, Application of ELDOR in electron-spin echo for paramagnetic center space distribution in solids, Fiz. Tverd. Tela. 23 (1981) 975–982.
[8] G. Jeschke, A. Bender, H. Paulsen, H. Zimmermann, A. Godt, Sensitivity enhancement in pulse EPR distance measurements, J. Magn. Reson. 169 (2004) 1–12.
[9] O. Schiemann, N. Piton, Y. Mu, G. Stock, J.W. Engels, T.F. Prisner, A PELDOR-based nanometer distance ruler for oligonucleotides, J. Am. Chem. Soc. 126 (2004) 5724–5729.
[10] A. Weber, O. Schiemann, B. Bode, T.F. Prisner, PELDOR at S- and X-band frequencies and the separation of exchange coupling from dipolar coupling, J. Magn. Reson. 157 (2002) 277–285.
[11] G. Jeschke, A. Koch, U. Jonas, A. Godt, Direct conversion of EPR dipolar time evolution data to distance distributions, J. Magn. Reson. 155 (2002) 72–82.
[12] G. Jeschke, V. Chechik, P. Ionita, A. Godt, H. Zimmermann, J. Banham, C.R. Timmel, D. Hilger, H. Jung, DeerAnalysis2006—a comprehensive software package for analyzing pulsed ELDOR data, Appl. Magn. Reson. 30 (2006) 473–498.
[13] J. Weese, A reliable and fast method for the solution of Fredholm integral equations of the first kind based on Tikhonov regularization, Comp. Phys. Commun. 69 (1992) 99–111.
[14] G. Jeschke, Distance measurements in the nanometer range by pulse EPR, Chem. Phys. Chem. 3 (2002) 927–932.
[15] M. Persson, J.R. Harbridge, P. Hammarstrom, R. Mitri, L.-G. Martensson, U. Carlsson, G.R. Eaton, S.S. Eaton, Comparison of electron paramagnetic resonance methods to determine distances between spin labels on human carbonic anhydrase II, Biophys. J. 80 (2001) 2886–2897.
[16] W.R. Fiori, S.M. Miick, G.L. Millhauser, Increasing sequence length favors alpha-helix in alanine-based peptides: evidence for a length-dependent structural transition, Biochemistry 32 (1993) 11957–11962.
[17] A. Abragam, The Principles of Nuclear Magnetism, OUP, 1961.
[18] H.-J. Steinhoff, Methods for study of protein dynamics and protein–protein interaction in protein–ubiquitination by electron paramagnetic resonance spectroscopy, Frontiers in Bioscience 7 (2002) 97–110.
[19] A.V. Kulikov, G.I. Likhtenstein, E.G. Rosantev, V.I. Suskina, A.B. Shapiro, On possible determination of distances between functional groups of protein by the method of spin labels, Biofizika 17 (1972) 42–48.
[20] J.H. van Vleck, The dipolar broadening of magnetic resonance lines in crystals, Phys. Rev. 74 (1948) 1168–1183.
[21] G.E. Pake, Nuclear resonance absorption in hydrated crystals: fine structure of the proton line, J. Chem. Phys. 16 (1948) 327–336.
[22] G. Jeschke, Determination of the nanostructure of polymer materials by electron paramagnetic resonance spectroscopy, Macromol. Rapid Commun. 23 (2002) 227–246.
[23] G.I. Likhtenstein, Spin Labeling Methods in Molecular Biology, Wiley, New York, 1976.
[24] N.-K. Kim, A. Murali, V.J. DeRose, A distance ruler for RNA using EPR and site-directed spin labeling, Chem. Biol. 11 (2004) 939–948.
[25] P.C. Hansen, Rank-Deficient and Discrete Ill-Posed Problems: Numerical Aspects of Linear Inversion, SIAM, Philadelphia, 1998.
[26] P.C. Hansen, Regularization Tools Version 3.1, 1998.
[27] J. Skilling, R.K. Bryan, Maximum entropy image reconstruction: general algorithm, Mon. Not. R. Astr. Soc. 211 (1984) 111–124.
[28] Y.-W. Chiang, P.P. Borbat, J.H. Freed, Maximum entropy: a complement to Tikhonov regularization for determination of pair distance distributions by pulsed ESR, J. Magn. Reson. 177 (2005) 167–179.
[29] A.G. Maryasov, Y.D. Tsvetkov, Formation of the pulsed electron–electron double resonance signal in the case of a finite amplitude of microwave fields, Appl. Magn. Reson. 18 (2000) 583–605.
[30] A.D. Milov, B.D. Naumov, Y.D. Tsvetkov, The effect of microwave pulse duration on the distance distribution function between spin labels obtained by Peldor data analysis, Appl. Magn. Reson. 26 (2004) 587–599.
[31] S. Stoll, A. Schweiger, EasySpin, a comprehensive software package for spectral simulation and analysis in EPR, J. Magn. Reson. 178 (2006) 42–55.
[32] A. Schweiger, G. Jeschke, Principles of pulse electron paramagnetic resonance, first ed., OUP, Oxford, 2001.
[33] J.E. Banham, Exploring long range structure in chemical and biological systems using electron paramagnetic resonance, D. Phil. thesis, Oxford, 2006.
[34] I.J. Day, Real-time NMR of the transient states of proteins, D.Phil. thesis, Oxford University, Oxford, 2004.
[35] www.cambridgesoft.com.
[36] A.I. Kokorin, K.I. Zamarayev, G.L. Grigoryan, V.P. Ivanov, E.G. Rozantsev, Measurement of the distances between the paramagnetic centres in solid solutions of nitroxide radicals, biradicals and spin-labelled proteins, Biofizika 17 (1972) 34–41.
[37] P.P. Borbat, J.H. Freed, Measuring distances by pulsed dipolar ESR spectroscopy: spin-labeled histidine kinases, Methods Enzymol. 423 (2007) 52–116.
[38] K. Nakanishi, N. Berova, R.W. Woody (Eds.), Circular Dichroism Principles and Applications, VCH, New York, 1994.
[39] B. Forood, E.J. Feliciano, K.P. Nambiar, Stabilization of alpha-helical structures in short peptides via end capping, Proc. Natl. Acad. Sci. USA 90 (1993) 838–842.
[40] M.C. Manning, R.W. Woody, Theoretical CD studies of polypeptide helices: examination of important electronic and geometric factors, Biopolymers 31 (1991) 569–586.
[41] D.S. Wishart, B.D. Sykes, F.M. Richards, The chemical shift index: a fast and simple method for the assignment of protein secondary

structure through NMR spectroscopy, Biochemistry 31 (1992) 1647–1651.
[42] B.R. Brooks, R.E. Bruccoleri, B.D. Olafson, D.J. States, S. Swaminathan, M. Karplus, CHARMM: a program for macromolecular energy, minimization, and dynamics calculations, J. Comput. Chem. (1983) 187–217.
[43] A.D. Mackerell, D. Bashford, R.L. Bellott, R.L. Dunbrack, J.D. Evanseck, M.J. Field, S. Fischer, J. Gao, H. Guo, S. Ha, D. Joseph-McCarthy, L. Kuchnir, K. Kuczera, F.T.K. Lau, M. Schelnkrich, J.C. Smith, R. Stote, J. Straub, M. Watanabe, J. Wiorkieqicz-Kuczera, D. Yin, M. Karplus, All-atom empirical potential for molecular modelling and dynamics studies of proteins, J. Phys. Chem. B 102 (1998) 3586–3616.
[44] M.K. Bowman, A.G. Maryasov, Dynamic phase shifts in nanoscale distance measurements by double electron electron resonance (DEER), J. Magn. Reson. 185 (2007) 270–282.